Effects of Interpolation on Segmentation in Cell Imaging

Arianny Coca-Rodríguez[1] and Juan V. Lorenzo-Ginori[2]

[1] Centro de Investigaciones Biomédicas, Universidad Médica "Serafín Ruiz de Zárate" de Villa Clara, Santa Clara, Cuba

[2] Centro de Estudios de Electrónica y Tecnologías de la Información, Facultad de Ingeniería Eléctrica, Universidad Central "Marta Abreu" de Las Villas, Santa Clara, Cuba

ariannycr@ucm.vcl.sld.cu, juanl@uclv.edu.cu

Abstract. In digital image processing and computer vision applications for microscopy imaging, calculating image features is a frequent task. Features related to intensity, color and morphology are used to classify cells and other objects. The precision of segmentation influences the calculated feature values and can affect the results of classification. Therefore, achieving a high precision in segmentation is very important. In this work, the effects of interpolation on the precision of image segmentation were studied using instances of cell microscopy images and different interpolation and segmentation methods. The goal was to determine quantitatively to what extent improvements in segmentation precision can be obtained through previous interpolation of the images. This effect can be particularly important for small objects, whose images might be deteriorated due to limitations in the camera's resolution. The results show that an improvement in the precision of segmentation can be obtained by previously interpolating the images.

Keywords. Interpolation, segmentation, cell imaging.

Efectos de la interpolación sobre la segmentación en imaginología celular

Resumen. En las aplicaciones del procesamiento digital de imágenes y la visión computacional para imágenes de microscopía, el cálculo de rasgos de las imágenes es una tarea frecuente. Rasgos relacionados con la intensidad, el color y la morfología, son utilizados para clasificar células y otros objetos. La precisión de la segmentación influye sobre los valores calculados para los rasgos y puede afectar los resultados de la clasificación. Por tanto, es muy importante alcanzar una alta precisión en la segmentación. En este trabajo fueron estudiados los efectos de la interpolación sobre la precisión de la segmentación, utilizando ejemplos de imágenes de microscopía celular y diferentes métodos de interpolación y de segmentación. El objetivo fue determinar en forma cuantitativa en qué medida se obtienen mejoras en la precisión de la segmentación mediante una interpolación previa de las imágenes. Este efecto puede ser particularmente importante para objetos pequeños, cuyas imágenes podrían sufrir deterioro debido a limitaciones en la resolución de la cámara. Los resultados muestran que es posible obtener una mejora en la precisión de la segmentación mediante la interpolación previa de las imágenes.

Palabras clave. Interpolación, segmentación, imaginología celular.

1 Introduction

In the applications of digital image processing and computer vision to microscopy imaging, image classification based on their features is a frequent task. In this case, the quality of the segmentation results is a very important issue. Intensity and color measures, objects' dimensions and forms (morphology), and other characteristics are examples of features used for classification purposes of cells and other objects. In many cases, the contours established by the segmentation process can have a direct influence on the calculated feature values, particularly those related to the amount and location of pixels that the objects can encompass in the digital image. Therefore, the results of segmentation may be determinant in the results of an automatic classification process. Achieving a high precision

in the segmentation of cells or other objects of interest within those images constitutes therefore an essential issue.

In this work, the effects of interpolation on the quality of segmentation were studied for this class of images. The goal was contributing to improve the reliability of the classification processes in cell imaging using computational methods. The research performed was specifically intended to determine if an improvement in the precision of segmentation can be obtained through previous interpolation, and in this case to quantify it by analyzing comparatively the effects of different interpolation methods.

An important motivation for this research is that the digital microscopy images may include small objects whose contours and morphological characteristics, for a specific magnifying, might be not very well represented in the digital image due to limitations of the camera's resolution. The hypothesis that motivated this work is that it is possible to obtain an improvement in the quality of segmentation in these cases if the image is previously interpolated.

1.1 Interpolation

To the effects of this analysis, interpolation is to be understood as a process in which the sampling rate of the digital image is incremented, determining the intensity values for the new pixels that will be inserted within the original ones. When the number of pixels per unit area is incremented, the spatial resolution can be improved, whenever the image had been sampled originally at a high enough rate in order to avoid the aliasing phenomenon. Among various well known interpolation methods we can mention the following, which were selected to be applied in this study:

- Bilinear,
- Bicubic,
- Interpolation with splines.

In bilinear interpolation, the pixel value is a weighted mean of the intensity values, corresponding to four pixels in a 2X2 neighborhood. This procedure can cause some blur in the image due to the mean value calculation involved.

In the bicubic interpolation, the interpolated pixels are weighted mean values in 4X4 neighborhoods, and tend to produce smoothed contours [4].

The term spline makes reference to a wide class of functions which are employed in applications requiring data interpolation or curve smoothing. Splines are employed in one or several dimensions and are particularly useful in image interpolation [8].

Spline interpolation consists actually in a family of methods including:

- Cubic splines,
- Smoothing splines,
- Least-Square-Approximations.

1.2 Segmentation

Image segmentation is defined as an automated or semi-automated process by means of which the structures of interest in an image are delineated and separated from the background [4]. The level of subdivision of details during segmentation is determined by the application's goal, and the segmentation process ends when the objects of interest had been isolated.
In this work, the study was realized using two well-known segmentation methods: Otsu's algorithm and the watershed transform (WT).

Otsu's algorithm [7] is used for grayscale image segmentation, in which the images include, for example, high intensity (clear) objects in the foreground and exhibit a low intensity, darker background. Here the intensities of pixels in the image (foreground and background objects) tend to have a bimodal histogram. Foreground and background pixels can be separated therefore by selecting an appropriate intensity threshold and performing the corresponding comparison and classification process.

The Otsu's algorithm is based in maximizing a statistical measure called "between-class variance". A threshold's optimum value is obtained, which provides the best separation between classes in terms of the intensity values of the objects to be segmented and the image background.

WT is a segmentation method based in morphological grayscale image processing which

is realized on a three-dimensional representation of the image's intensity as a surface [12].

The WT is usually applied to the gradient of the image to be segmented, which can be defined both for grayscale and color images. It is also frequently applied to the images obtained from the calculation of the distance transform for binary images. The results for real images lead usually to the so-called over-segmentation phenomenon. This is usually due to the presence of multiple local minima in the images, related to the presence of noise and other local irregularities in the gradient image. A solution for this problem is the use of markers in order to limit the number of segmentation regions. These markers are imposed on the objects to be segmented and serve to indicate, respectively, the inner and outer regions of the objects' contours.

The success of WT segmentation depends mainly upon the markers' characteristics and the quality of the gradient image. WT results are independent of the markers' locations whenever they had been appropriately placed inside and outside the objects, and the gradients associated to the object's contours are significant when compared to the gradient values inside them.

1.3 Evaluating the Quality of Segmentation

The existence of a large number of image segmentation algorithms has determined that various techniques had been developed to evaluate and compare their performance [9]. The case of cell segmentation in microscopy images has been studied specifically as well [1]. These segmentation evaluation methods can be especially useful to the effects of this research which pursues comparing the segmentation results for different interpolation alternatives. This comparison has been realized here using statistical hypothesis testing.

Considering the above mentioned ideas, this work starts from the hypothesis that it is possible to improve the quality of segmentation if the image is previously interpolated. The objective here is therefore measuring quantitatively the effects, if any, of using different interpolation methods before segmentation in terms of segmentation quality. These tests were realized specifically applying the Otsu's method and the WT to cell microscopy images.

The organization of this paper is as follows. Section 2 describes the materials and methods used in terms of the images employed, experiments performed and segmentation evaluation methods used. Section 3 exhibits the results by means of figures and tables and discusses them. Finally, Section 4 presents the conclusions.

2 Materials and Methods

2.1 Characteristics of the Images Employed in this Study

This study was realized using two sets of ten images each: one set is composed by synthetic images generated using an erythrocyte simulation algorithm [6] and the other is composed of ten images drawn from an atlas of hematology [5]. The digital images that appear in the latter were obtained from human blood smears and all of them are represented in the RGB color space. Examples of the synthetic images and their corresponding segmentation mask (the binary image resulting from segmentation in which pixels belonging to the objects of interest have the binary level 1), as well as from the real images,

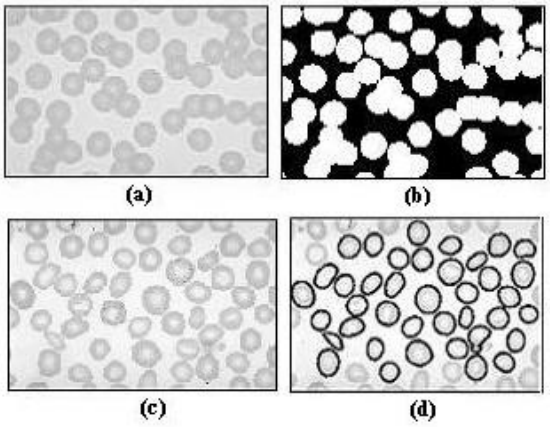

Fig. 1. Images employed: (a) synthetic image, (b) segmentation mask from image (a), (c) image from the database (basophilic stippling), (d) the corresponding segmented grayscale image using Otsu's thresholding, with the contours in bold

together with a segmentation result with cell borders highlighted, are shown in Fig. 1.

2.2 Experiments

The block diagram depicted in Fig. 2 illustrates the experiments realized to investigate the effects of interpolation on the segmentation quality. These were performed in a desktop computer Pentium IV with 1 GB RAM. Starting from an image with a given resolution, another image was simulated, which was equivalent to the one that would be obtained with a lower resolution camera. Resolution was lowered by some factor as follows.

In each case, the original image, to the effects of this study, was considered as the high resolution (HR) image. From this image, a new image called HR_modified was simulated, which has a number of rows and columns divisible by 2 or by 4. These were the factors used to reduce the numbers of pixels by rows and columns (and later to interpolate the image). To obtain this result, the minimum possible number of border rows and columns were deleted from the digital image matrix, in order to keep the image as unaltered as possible.

After this, a simulated image with lowered resolution was created. This was done by calculating the mean value of the pixels in a 2X2 or 4X4 neighborhood, according to the desired reduction of the resolution. The intensity value in the low-resolution pixels corresponding to the neighborhoods was substituted by the calculated mean, as shown in Fig. 3 and described in [11], where it is used in the context of a study on super-resolution interpolation techniques. In order to generate the simulated, lowered resolution images, a function called *low_res* was created. This function uses three input parameters:

- Ahr: original image, considered as having high resolution.
- mfact: numerical value (integer) by which the number of rows of the original image will be reduced.
- nfact: same as mfact, but related to the number of columns. In this work mfact=nfact, leading to 2X2 and 4X4 neighborhoods. As a result from this function, the following results are obtained:
- Ahr_modified: conversion of the original image to grayscale (in case of necessity) and reduction of the number of rows and columns to the highest value which is divisible by the factors chosen. Obtaining this image is represented in Fig. 2 by the block named HR_modified.
- Alr: low resolution image, corresponding to the chosen factors selected by the user. It corresponds to the LR blocks in Fig. 2.

In Fig. 2, the branch labeled as 3 in the block diagram contains the operations that are to be performed on the HR modified image in order to obtain the ground-truth used to evaluate the quality of segmentation. In the case of synthetic images, the ground-truth is supplied together with each synthetic image and it is simply read and scaled. In the case of the real images drawn from the database, the HR modified image is

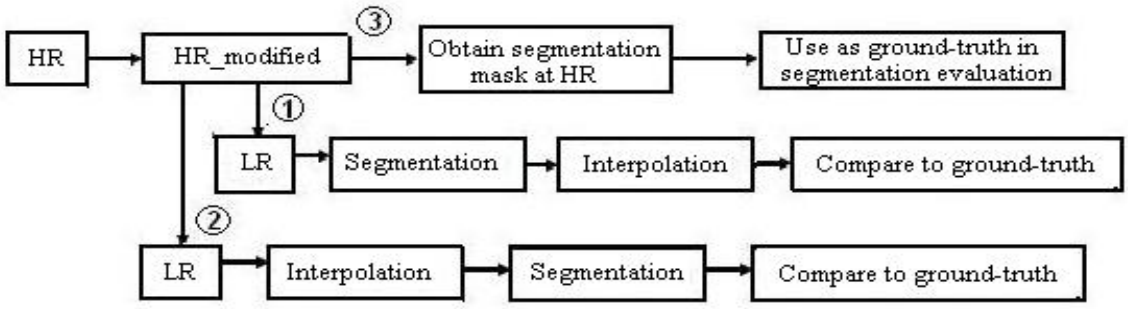

Fig. 2. Block diagram showing the procedure used to evaluate the effects of interpolation on the segmentation process, for any segmentation algorithm

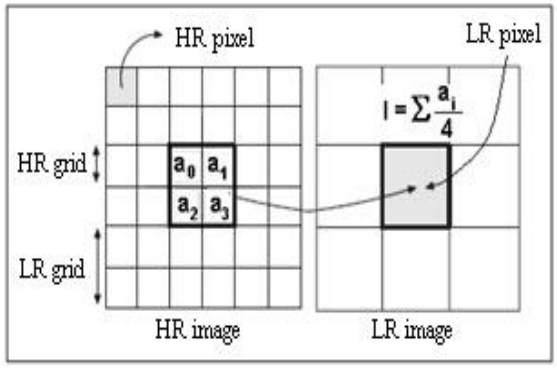

Fig. 3. Obtaining a simulated low-resolution image

segmented (using either the Otsu's algorithm or the WT) in order to obtain the ground-truth. This is considered here as the "true" segmentation result for having been obtained at high resolution. Notice that for simulated images, the segmentation for interpolated or low resolution images are both compared in this work to the synthetic ground-truth. On the other hand, for real images from the database, the segmentation results at low resolution and for interpolated images are compared to the ground-truth obtained by segmenting the image at high resolution.

Branches 1 and 2 in Fig. 2 correspond, respectively, to the experiments performed. In Experiment 1, the first step consisted in obtaining the low resolution image LR using the function *low_res*, then its segmentation was performed at low resolution and the result was interpolated, obtaining an image of the same size as the ground-truth.

Finally, the quality of segmentation was evaluated by comparing the obtained image with the ground-truth.

In Branch 2 of Fig. 2 (Experiment 2), the low resolution image was interpolated by the same factor previously used to simulate the reduced resolution effect in the image. Then it was segmented and the resulting image was compared to the ground-truth to evaluate the quality of segmentation.

Notice that Experiments 1 and 2 differ only in the order in which interpolation and segmentation are performed.

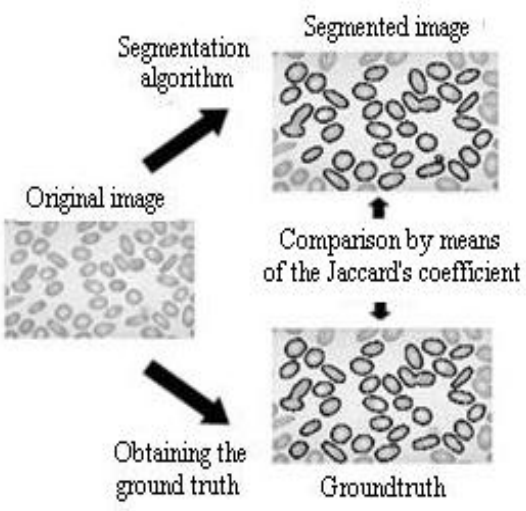

Fig. 4. Supervised evaluation of the segmentation results by comparing to ground-truth

2.3 Evaluating the Quality of Segmentation

To evaluate the results of segmentation, a binary mask was obtained firstly by segmenting the ground-truth. The binary segmentation masks obtained from Experiments 1 and 2 were then compared to the ground-truth mask. Fig. 4 illustrates this process. The ground-truth was obtained following Branch 3 in Fig. 2, and the segmentation masks following Branches 1 and 2. The fact, that only the effects of interpolation on segmentation are those to be evaluated, determined that the segmentation mask associated to the high resolution image was used as ground-truth for the case of the real images from the database.

The measure used in this work to compare binary masks was the Jaccard's coefficient, widely used in various works previously reported in the literature, an example of which is found in [3].

The Jaccard's coefficient is expressed as

$$J(A,B) = \frac{|A \cap B|}{|A \cup B|}, \quad 0 \leq J(A,B) \leq 1, \tag{1}$$

where $|\bullet|$ is the cardinality of the set between bars. In terms of binary images, the Jaccard's

coefficient is the quotient between the numbers of pixels in the sets' intersection and in the sets' union, respectively, corresponding to the segmented objects (actually their binary masks) in the images to be compared. If the *J* value obtained is 1, the coincidence between the corresponding objects in the images is perfect, and if it is zero, the objects do not overlap at all, the practical cases lying in between. The *J* coefficient for each pair of objects is usually calculated pairing the labelled ground-truth and the final images resulting from segmentation. The objects present in both images are identified by automatically labelling them.

When the purpose of segmentation is oriented to realize further computational pattern recognition, it is convenient to suppress the cells that touch the image borders, leaving only the entire cells that exhibit their natural forms. This elimination was performed in this work using morphological signal processing techniques [10] applied to the binary masks obtained from the segmentation process.

When using this technique, differences in labelling of objects or cells can appear between the ground-truth and the segmented images, due to the presence of an unequal number of objects in them. This might occur because when the resolution is lowered to obtain the LR images, some objects that did not touch the borders can become connected to others that do touch them, causing their deletion as unique combined border-touching objects. This situation determined that when calculating the *J* coefficient, the objects could not be paired correctly according to their respective labelling numbers.

To deal with this situation, another procedure was used in this work instead, based in morphological operations applied to the segmentation masks. An outline of this is presented below:

1. Label the ground-truth segmentation mask after deleting the small objects considered as artifacts (through morphological area-opening) as well as the border-touching objects. Instead of matching labels, now the algorithm looks for a matching object in the resulting segmentation mask.
2. Determine the sets' intersection and the sets' union between the ground-truth mask and the segmentation mask from the segmented image to evaluate. The resulting intersection set for each object in the image will be a non-empty set only if the ground-truth finds a corresponding object in the evaluated image, i.e., if the latter was not deleted for having been connected at low resolution to a border-touching object.
3. Perform a morphological reconstruction using the intersections as markers and the unions as masks. Notice that in case that the intersection is an empty set, the same will occur with the marker and consequently with the reconstruction result. In other cases, the reconstruction will result in the union set for each object.
4. Calculate the *J* coefficients for each object using Equation 1. For each object in the ground-truth, *J* will be indeterminate whenever the intersection is an empty set, and correctly calculated in other cases. The number of indeterminate cases is associated with missing objects due to lowered resolution, as it was explained above. This can serve as an additional (negative) indicator of the quality of segmentation. Indeterminate cases were denoted here as NaN's (not a number).

As a final step in evaluating the segmentation quality, a statistical analysis was performed using non-parametric tests on the mean values of the *J* coefficients for the two employed sets (simulated and real) of ten images each [13].

Firstly, in order to determine if there were significant statistical differences between the results of Experiments 1 and 2, the Wilcoxon signed rank test was employed. Here we were working with two sets of ten paired images each, with a relatively high number of objects (cells) contained in them. The possible differences among the three interpolation methods employed were also analyzed using the Friedman test. In this case, the null hypothesis was that there are no significant differences among the results for the three methods (i.e., they have distributions with zero differences of the medians.) The alternative hypothesis was that at least one of the

interpolation methods has a distribution of *J* that differs from the others. The Wilcoxon test was employed as a post-hoc analysis. These statistical tests were performed using SPSS 15.0 for Windows, and the significance level used was 0.05.

In this research, the following combinations of interpolation and segmentation methods were used in the experiments:

1. Resolution reduced by a factor of 2 in each axis, segmentation by Otsu's algorithm and the WT, both for the three interpolation methods: bilinear, bicubic and splines (six alternatives in total).
2. Same as in the previous case, but with resolution reduced by a factor of 4 in each axis. This meant again six alternatives.

3 Results and Discussion

The results obtained for the various alternatives tested are summarized below.

3.1 Obtaining the Ground-Truth

The ground-truth image was provided together with the simulated images or obtained by segmenting directly the high resolution real images, as it was explained before. This function returns, aside from the Alr (LR) image, the image Ahr_modified, as it was explained in section 2.2. For this case, Fig. 5 shows an example of the ground-truth image that was obtained for a resolution reduction factor 2, with Otsu's segmentation of the image converted to grayscale and deletion of border-touching cells. This procedure was realized for the ten real images employed.

Notice that in the lower left corner, an object was deleted because it became connected to a border-touching object at low resolution. Such objects are the ones that lead to NaN results when evaluating *J.*

The total number of *J* coefficient's values that is obtained for a given image is equal to the number of objects in the ground-truth image without artifacts. Labeling of objects is represented in Fig. 5 by their color.

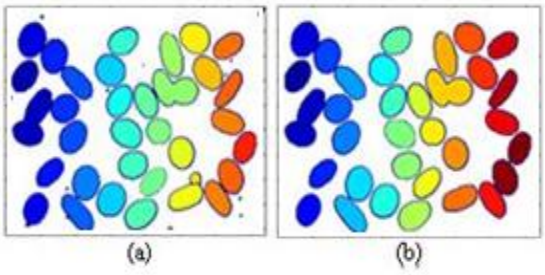

Fig. 5. Obtaining the ground-truth: (a) labeled with small artifacts, it has 95 objects, (b) artifacts cleaned, 33 objects remaining

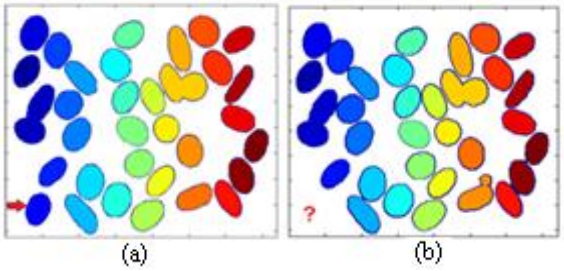

Fig. 6. Images compared in Experiment 1, final step. Notice that the object indicated with an arrow in the ground-truth (a) is missing in the result (b)

3.2 Results of Experiment 1

The images corresponding to the comparison made in the last step of Experiment 1 are shown in Fig. 6, for resolution reduction factor of 2, Otsu's segmentation and bicubic interpolation by the same factor. Notice that in the lower left corner an object was deleted because it became connected to a border-touching object at low resolution. These are the objects that lead to a NaN result when evaluating *J.* The total number of *J* coefficient values that is obtained for a given image is equal to the number of objects in the ground-truth image without artifacts.

3.3 Results of Experiment 2

Similarly to Experiment 1, using the same methods and changing only the order in which interpolation and segmentation were performed, the image (b) shown in Fig. 7 was obtained. The

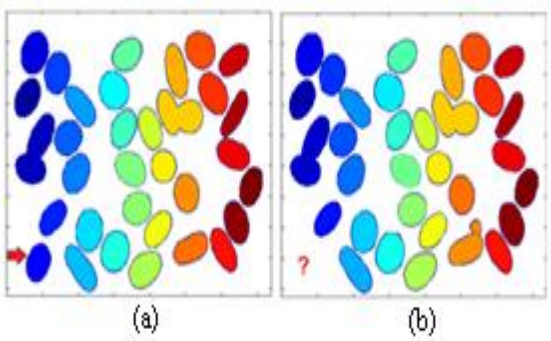

Fig. 7. Images to be compared, corresponding to the final step in Experiment 2 indicating a missing object

differences, when comparing Fig.7(b) to Fig. 6 are not easily noticeable by the naked eye, but the measured *J* values obtained were indeed different.

The images, that were compared, generated a list of 33 values of *J* in this example. The mean values for *J* for each of the 10 images were calculated (obviously discarding the NaN's). The results are shown in Table 1 for Experiments 1 and 2, together with the number of NaN's obtained in each case. Notice that for most cell morphologies, results from Experiment 2 were better than those from Experiment 1.

3.4 Statistical Analysis

In this section, we present the results of the statistical analysis performed on the data that were gathered in 12 tables analogous to Table 1.

Firstly it was determined if interpolating before segmenting meant any advantage, i.e., we investigated if results from Experiment 2 were superior to those from Experiment 1. Tables 2 and 3 show the results in terms of the ranks, for the Wilcoxon signed ranks test, applied to each set of *J* mean values from Experiment 2, paired to those from Experiment 1, for synthetic and real images and for Otsu's and WT segmentation algorithms, respectively.

Table 4 and Table 5 show the hypothesis testing results from Experiments 1 and 2, both for simulated and real images. We can appreciate in Table 4 that the null hypothesis (recall that it means that results from Experiments 1 and 2 are equivalent) is not rejected in any case for resolution reduction/interpolation factor equal to 2, although the probabilities are relatively close to the significance level chosen (0.05). However, for a factor of 4, the null hypothesis was rejected for bicubic and spline interpolation and is close to the threshold for the bilinear case. The results for WT segmentation showed a significant advantage of Experiment 2 against 1, for all the interpolation methods, for both factors 2 and 4. In regard of Table 5 (real images), the results are similar to those obtained for synthetic images. Notice that the ground truth was in this case the set segmentation masks at high-resolution. A decrement in the number NaN results was systematically observed for Experiment 2 in comparison to Experiment 1 in all cases, and an example of this is shown in Table 1.

Table 1. Results of Experiments 1 and 2 for bicubic interpolation, Otsu's segmentation and resolution reduced by 2

Images from the database	Experiment 1 J/ No. of NaN*s	Experiment 2 J/ No. of NaN*s
Basophilic Stipling	0,971/ 3	0,992/ 2
Elliptocyte	0,968/ 1	0,989/ 1
Howell-Jolly's body	0,942/ 0	0,957/ 0
Leptocyte	0,964/ 1	0,971/ 0
Malaria	0,972/ 0	0,990/ 0
Pappenheimer's body	0,968/ 0	0,989/ 0
Poikilocyte	0,965/ 0	0,939/ 0
Spherocyte	0,969/ 0	0,992/ 0
Tear Drop Cell	0,964/ 0	0,986/ 0
Thalassemia	0,914/ 0	0,938/ 0

Table 2. Wilcoxon signed rank test to compare Experiments 1 and 2 for Otsu's segmentation: ranks

Wilcoxon test ranks		Synthetic images			Real images from the database		
		N	Mean Rank	Sum of Ranks	N	Mean Rank	Sum of Ranks
Experim 2 vs. Experim 1 Bilinear Factor=2	Negative Ranks	2	1.50	3.00	1	10.00	10.00
	Positive Ranks	8	6.50	52.00	9	5.00	45.00
	Ties	0			0		
	Total	10			10		
Experim 2 vs. Experim 1 Bicubic Factor=2	Negative Ranks	0	.00	.00	1	10.00	10.00
	Positive Ranks	10	5.50	55.00	9	5.00	45.00
	Ties	0			0		
	Total	10			10		
Experim 2 vs. Experim 1 Splines Factor=2	Negative Ranks	0	.00	.00	2	5 50	11.00
	Positive Ranks	10	5.50	55.00	8	5.50	44.00
	Ties	0			0		
	Total	10			10		
Experim 2 vs. Experim 1 Bilinear Factor=4	Negative Ranks	1	1.00	1.00	2	4.50	9.00
	Positive Ranks	9	6.00	54.00	8	5.75	46.00
	Ties	0			0		
	Total	10			10		
Experim 2 vs. Experim 1 Bicubic Factor=4	Negative Ranks	1	10.00	10.0	0	0.00	0.00
	Positive Ranks	9	5.00	45.00	10	5.50	55.00
	Ties	0			0		
	Total	10			10		
Experim 2 vs. Experim 1 Splines Factor=4	Negative Ranks	0	.00	.00	0	0.00	0.00
	Positive Ranks	10	5.50	55.00	10	5.50	55.00
	Ties	0			0		
	Total	10			10		

Negative ranks: *J*/ Experiment 2 < *J*/ Experiment 1, Positive ranks: *J*/ Experiment 2 > *J*/ Experiment 1, Ties: *J*/ Experiment 2 = *J*/ Experiment 1

Table 3. Wilcoxon signed rank test, comparing Experiments 1 and 2 for WT segmentation: ranks

Wilcoxon test ranks		Synthetic images			Real images from the database		
		N	Mean Rank	Sum of Ranks	N	Mean Rank	Sum of Ranks
Experim 2 vs. Experim 1 Bilinear Factor=2	Negative Ranks	0	.00	.00	0	.00	.00
	Positive Ranks	10	5.50	55.00	10	5.50	55.00
	Ties	0			0		
	Total	10			10		
Experim 2 vs. Experim 1 Bicubic Factor=2	Negative Ranks	0	.00	.00	0	.00	.00
	Positive Ranks	10	5.50	55.00	10	5.50	55.00
	Ties	0			0		
	Total	10			10		
Experim 2 vs. Experim 1 Splines Factor=2	Negative Ranks	0	.00	.00	0	.00	.00
	Positive Ranks	10	5.50	55.00	10	5.50	55.00
	Ties	0			0		
	Total	10			10		
Experim 2 vs. Experim 1 Bilinear Factor=4	Negative Ranks	1	1.00	1.00	1[j]	.00	.00
	Positive Ranks	9	6.00	54.00	9	5.50	55.00
	Ties	0			0		
	Total	10			10		
Experim 2 vs. Experim 1 Bicubic Factor=4	Negative Ranks	0	.00	.00	0	.00	.00
	Positive Ranks	10	5.50	55.00	10	5.50	55.00
	Ties	0			0		
	Total	10			10		
Experim 2 vs. Experim 1 Splines Factor=4	Negative Ranks	0	.00	.00	0	.00	.00
	Positive Ranks	10	5.50	55.00	10	5.50	55.00
	Ties	0			0		
	Total	10			10		

Negative ranks: *J*/ Experiment 2 < *J*/ Experiment 1, Positive ranks: *J*/ Experiment 2 > *J*/ Experiment 1, Ties: *J*/ Experiment 2 = *J*/ Experiment 1

Table 4. Statistics from the Wilcoxon signed rank test, comparing results from Experiments 1 and 2, for simulated images

Method		Exp 2 vs.1 Bilinear factor: 2	Exp 2 vs.1 Bicubic factor: 2	Exp 2 vs.1 Splines factor: 2	Exp 2 vs. 1 Bilinear factor: 4	Exp 2 vs.1 Bicubic factor: 4	Exp 2 vs.1 Splines· factor: 2
Otsu	Z	-1.784[a]	-1.785[a]	-1.682[a]	-1.886[a]	-2.803[a]	-2.803[a]
	Exact Sig. (2- tailed)	.084	.080	.105	.054	.002	.002
Watershed Transform	Z	-2.803[a]	-2.803[a]	-2.803[a]	-2.701[a]	-2.803[a]	-2.803[a]
	Exact Sig. (2- tailed)	.002	.002	.002	.004	.002	.002

a. Based on negative ranks.

Table 5. Statistics of the Wilcoxon signed rank test to compare results from Experiments 1 and 2, for real images

Method		Exp 2 vs.1 Bilinear factor: 2	Exp 2 vs.1 Bicubic factor: 2	Exp 2 vs.1 Splines factor: 2	Exp 2 vs. 1 Bilinear factor: 4	Exp 2 vs.1 Bicubic factor: 4	Exp 2 vs.1 Splines· factor: 2
Otsu	Z	-1.784[a]	-1.785[a]	-1.682[a]	-1.886[a]	-2.803[a]	-2.803[a]
	Exact Sig. (2- tailed)	.084	.080	.105	.064	.002	.002
Watershed Transform	Z	-2.803[a]	-2.803[a]	-2.803[a]	-2.803[a]	-2.803[a]	-2.803[a]
	Exact Sig. (2- tailed)	.005	.005	.005	.005	.005	.005

a. Based on negative ranks.

Table 6 illustrates the results for the Friedman test to determine if there were significant differences among the performances of the three interpolation methods, in regard to segmentation quality. The test was applied for watershed transform segmentation, interpolation factor 4 and real images, as this condition tends to make a clearer difference between the results from Experiments 1 and 2. The largest rank is associated here to a better algorithm performance, which corresponded in this case to bicubic interpolation. A post-hoc analysis using the Wilcoxon test confirmed this result.

In regard of computer times for interpolation, it was observed, as shown in Table 7, that the bilinear method was the fastest, followed by the bicubic one. The latter was almost equally fast, but with a better segmentation quality and this suggests that using it would be a good compromise between precision and speed.

4 Conclusions

Our study was realized with the purpose of determining the possible advantages, in regard of segmentation results that could be obtained, by performing an interpolation of the microscopy cell images before segmenting them. In order to accomplish this, two reference sets of ten cell images were employed: one composed by synthetic images together with their segmentation

Table 6. Results of the Friedman test to determine the best interpolation method (real images, watershed)

Experiment 2 Factor 4	Mean rank
Bilinear	1.60
Bicubic	2.90
Splines	1.50
Statistics	
N	10
Chi-square	12.2
Degrees of freedom	2
Exact Significance	0.001

Table 7. Computational load of the interpolation algorithms, in terms of computing time

Experiment 2	Time, s
Bilinear	0.018
Bicubic	0.027
Splines	0.121

mask, and the other by real images from a database. Lower resolution images were simulated from the reference images, and appropriate experiments were performed.

The segmentation quality was evaluated for two frequently used algorithms, Otsu's and the watershed transform, in terms of the Jaccard's coefficient between reference images at high resolution and the resulting segmented images. The results were analyzed using non-parametric statistical tests, and showed that in fact an improvement in the quality of segmentation was obtained when the images were previously interpolated, for both segmentation methods. In the experiments realized, it was observed that among the bilinear, bicubic and splines interpolation methods, the second one showed the most favorable results in terms of segmentation quality. These results were evidenced more clearly for the X4 factor used to reduce resolution and interpolating. Additionally, it was observed that the bilinear method was the fastest in regard of computer time.

The results obtained suggest the convenience of interpolating the microscopy images before segmentation in order to improve the precision of segmentation, as well as that this improvement might be more significant for a higher interpolation factor. This makes this procedure advisable whenever the resolution with which the images had been obtained is relatively limited and an increment in computational load is permissible. The obtained advantage can be useful when the task is to segment and classify small objects which were not very well delineated in the digital image due to a limited camera resolution. Future work will address an extension to evaluate other interpolation algorithms and segmentation methods to assess their behavior in the applications studied in this research.

Acknowledgements

The authors acknowledge B.Sc. (Biomed. Eng.) Lisdania Acea Mena for her collaboration in this work. This research received support from the Canadian International Development Agency (CIDA) Project "Biomedical Engineering Education in Cuba", Tier II-394-TT02-00. It also received support from the Institutional University Co-operation (IUC) program of the Flemish University Council (VLIR) and from the Center for Studies in Electronics and Information Technologies at Universidad Central "Marta Abreu" de Las Villas.

References

1. **Dima, A. A., Elliott, J.T., Filliben, J.J., Halter, M., Peskin, A., Bernal, J., Kociolek, M., Brady, M.C., Tang, H.C., & Plant, A.L. (2011).** Comparison of segmentation algorithms for fluorescence microscopy images of cells. *Cytometry Part A: the journal of the International Society for Analytical Cytology*, 79(7), 545–559.
2. **Dougherty, E.R. & Lotufo, R.A. (2003).** *Hands-on morphological image processing*. Belingham, Wash.: Spie Optical Engineering Press.
3. **Feng, G., Wang, S., & Liu, T. (2007).** A New benchmark for image segmentation evaluation.

Journal of Electronic Imaging, 16(3), 033011-1–033011-16.

4. **Gonzalez, R.C. & Woods, R.E. (2008).** *Digital image processing* (3rd ed.). Upper Saddle River, N.J.: Prentice Hall.
5. **Ichihashi, T., Naoe, T., Kuriyama, K., Sasada, M., & Ohno, R. (2009, November 24).** Atlas of Hematology. Retrieved from http://pathy.med.nagoya-u.ac.jp/atlas/doc/atlas.html.
6. **Moreno-Montes-de-Oca, A., Chinea-Valdés, L., & Lorenzo-Ginori, J.V. (2011).** Algoritmo para la Generación de Imágenes Sintéticas de Microscopía Celular formadas por Eritrocitos y Evaluación de Algoritmos de Segmentación*. V Latin American Congress on Biomedical Engineering (CLAIB 2011),* Habana, Cuba, *IFMBE Proceedings,* 33, 1031–1034*.*
7. **Otsu, N. (1979).** A threshold selection method from gray-level histograms. *IEEE Transactions onSystems, Man and Cybernetics*, 9(1), 62–66.
8. **Pratt, W.K. (2001).** *Digital Image Processing: PIKS inside* (3rd. ed.). New York: Wiley.
9. **Rosenberger, C., Chabrier, S., Laurent, H., & Emile, B. (2006).** Unsupervised and supervised image segmentation evaluation. In Zhang, Y.J. (Ed.). *Advances in image and video segmentation* (365–393). Hershey, PA: IRM Press.
10. **Soille, P. (2003).** *Morphological image analysis: principles and applications*. Berlin; New York: Springer.
11. **Park, S.C., Park, M.K., & Kang, M.G. (2003).** Super-resolution image reconstruction: a technical overview. *IEEE Signal Processing Magazine*, 20(3), 21–36.
12. **Vincent, L. & Soille, P. (1991).** Watersheds in digital spaces: An efficient algorithm based on immersion simulations. *IEEE Transactions on Pattern Analysis and Machine Intelligence*, 13(6), 583–598.
13. **Walpole, R.E., Myers, R.H., & Myers, S.L. (1999).** *Probabilidades y estadística para ingenieros* (6ta ed.). México: Prentice Hall Hispanoamericana.

Arianny Coca-Rodríguez, B.Sc., graduated as Biomedical Engineer from the Central University "Marta Abreu" de Las Villas (UCLV) in 2011. She currently works at the Center for Biomedical Research of the Medical University "Serafín Ruiz de Zárate" de Villa Clara, Santa Clara, Cuba, where she is a junior researcher. She is currently pursuing the M.Sc. degree in Signals and Systems at UCLV, in the area of digital image processing in cellular imaging.

Juan V. Lorenzo-Ginori, Ph.D., obtained the Dr. Tech. Sc. (Ph.D.) degree from UCLV in 1982. He is currently a Consultant Professor at the Electrical Engineering Faculty, Central University "Marta Abreu" de Las Villas. Dr. Lorenzo-Ginori has authored or co-authored a number of papers presented at national and international scientific conferences, as well as published more than 50 papers in refereed journals. He has also tutored several M.Sc. and Ph.D. theses. His current interests are the application of digital signal image in biomedical engineering, with emphasis in cellular and molecular imaging. Dr. Lorenzo-Ginori is member of the Academy of Science of the Republic of Cuba, Senior Member of the IEEE and fellow member of the Cuban Bioengineering Society.

Article received on 23/03/2013, accepted on 24/06/2013.